PCCP

RSC Publishing

PAPER

View Article Online
View Journal | View Issue

Thermal effects on electronic properties of CO/Pt(111) in water†

Cite this: *Phys. Chem. Chem. Phys.*, 2013, **15**, 13619

Sai Duan,[ab] Xin Xu,[c] Yi Luo,*[ad] Kersti Hermansson[a] and Zhong-Qun Tian[b]

Structure and adsorption energy of carbon monoxide molecules adsorbed on the Pt(111) surfaces with various CO coverages in water as well as work function of the whole systems at room temperature of 298 K were studied by means of a hybrid method that combines classical molecular dynamics and density functional theory. We found that when the coverage of CO is around half monolayer, *i.e.* 50%, there is no obvious peak of the oxygen density profile appearing in the first water layer. This result reveals that, in this case, the external force applied to water molecules from the CO/Pt(111) surface almost vanishes as a result of the competitive adsorption between CO and water molecules on the Pt(111) surface. This coverage is also the critical point of the wetting/non-wetting conditions for the CO/Pt(111) surface. Averaged work function and adsorption energy from current simulations are consistent with those of previous studies, which show that thermal average is required for direct comparisons between theoretical predictions and experimental measurements. Meanwhile, the statistical behaviors of work function and adsorption energy at room temperature have also been calculated. The standard errors of the calculated work function for the water–CO/Pt(111) interfaces are around 0.6 eV at all CO coverages, while the standard error decreases from 1.29 to 0.05 eV as the CO coverage increases from 4% to 100% for the calculated adsorption energy. Moreover, the critical points for these electronic properties are the same as those for the wetting/non-wetting conditions. These findings provide a better understanding about the interfacial structure under specific adsorption conditions, which can have important applications on the structure of electric double layers and therefore offer a useful perspective for the design of the electrochemical catalysts.

Received 11th April 2013,
Accepted 17th June 2013

DOI: 10.1039/c3cp51545a

www.rsc.org/pccp

1 Introduction

As an important branch of chemistry, electrochemistry has wide applications in industry and biology.[1,2] Exploring the structural details of the electric double layer (EDL) has always been the key issue in electrochemistry. For this purpose, many *in situ* techniques have been developed to probe the structure of EDL.[3] However, the structural details of EDL at the atomic level are still very difficult to obtain experimentally.[4,5] In this context, theoretical modeling of electrochemical systems is thus highly desirable.

Various theoretical models have been developed for EDL from the simplest Helmholtz model[6] to the more sophisticated models.[7] For instance, the model of Bockris, Devanathan and Muller for EDL has already taken into account the solvent dipole moments and their orientations.[8] In the last decade, more theoretical models for electrochemical systems have been proposed to consider the effects of the constant chemical potential,[9] the charged interface,[10,11] the computational hydrogen electrode,[12,13] the shifting of Fermi energy,[14,15] or the diffuse layer in EDL.[16,17] In these methods, although atomic resolution is achieved, the working temperature is always limited at 0 K. Obviously, practical electrochemical experiments usually take place at room temperature. The temperature difference between experiments and theoretical models leads to a big gap to fill when it comes to the interpretation of experimental results.

Platinum (Pt) is a widely used electrode that has great activities for electrocatalysis, especially in fuel cells.[18,19] It is

[a] *Department of Theoretical Chemistry and Biology, School of Biotechnology, Royal Institute of Technology, S-106 91 Stockholm, Sweden. E-mail: luo@kth.se; Fax: +46 (0)8 55378414; Tel: +46 (0)8 55378590*
[b] *State Key Laboratory of Physical Chemistry of Solid Surfaces and College of Chemistry and Chemical Engineering, Xiamen University, Xiamen 361005, P. R. China*
[c] *MOE Laboratory for Computational Physical Sciences, Department of Chemistry, Fudan University, Shanghai 200433, P. R. China*
[d] *Hefei National Laboratory for Physical Sciences at the Microscale, University of Science and Technology of China, Hefei, Anhui 230026, P. R. China*

† Electronic supplementary information (ESI) available: Optimized structures of the water–CO complex and calculated work functions of pure Pt(111) in a vacuum with different CO coverages. See DOI: 10.1039/c3cp51545a

well-known that carbon monoxide (CO) is a poisonous intermediate product in the Pt related fuel cells since CO can specifically adsorb on Pt surfaces.[20] The adsorption behavior of CO on Pt surfaces has been extensively studied both experimentally and theoretically.[21,22] Previous studies showed that the work functions (WFs) of CO/Pt(111) surfaces did not change significantly under ultra high vacuum conditions with different coverages of CO (θ).[23] On the other hand, for the model systems of CO/Pt(111) surfaces immersed into water, the WFs increased with the increase of θ.[21] This discrepancy is expected to be attributed to the interaction between water molecules and the specifically adsorbed CO/Pt(111) surfaces. As mentioned above, previous theoretical investigations were restricted to 0 K,[24,25] although a wide range of temperature was adopted for this three-component system in experiments.[26,27] Apparently, the gap between theoretical simulations (0 K) and experimental observations (finite temperature) also exists in the study of the CO/Pt(111) systems.

In the present work, we have investigated the CO/Pt(111) system in liquid water at room temperature using a hybrid theoretical approach that combines the classical molecular dynamics (MD) and the first principles methods to account for the thermal effects on the interfacial properties.[28] Within the framework of the classical MD, we can include the temperature effects without introducing the artificial mirror interactions between small supercells. The supercell employed in the classical MD is much larger than what is possible in the first principles MD simulations. From the trajectories generated by the classical MD, electronic properties of the evenly selected configurations were calculated at the density functional theory (DFT) level. We have shown in our previous study that the calculated WFs agreed very well with the experimental results.[28]

2 Computational details

The theoretically optimized lattice constant of bulk Pt at the generalized gradient approximation (GGA) DFT level by using Perdew–Burke–Ernzerhof (PBE) functional is 3.976 Å.[29] This result is in good agreement with the experimental value of 3.924 Å.[30] Three layers of the $p(5 \times 5)$ Pt(111) surface were used to represent the Pt(111) electrode. In the current study, 1, 5, 13, 20 and 25 CO molecules were adsorbed on the $p(5 \times 5)$ Pt(111) surface, corresponding to the θ of 4%, 20%, 52%, 80%, and 100%, respectively. All CO molecules were adsorbed on atop sites.[31] The detailed quasi-random patterns for CO are depicted in Fig. 1. 72 water molecules were added on the top of CO/Pt(111) surfaces to mimic the extremely dilute solutions. Periodic boundary conditions (PBC) were used for all dimensions. The z axis for the calculated supercell was set to be 50 Å to ensure that there is enough vacuum space between the two neighboring supercells.

The canonical ensemble (NVT) was used in the classical MD simulations by the Nosé–Hoover thermostat with a relaxation constant of 0.5 ps under 298 K.[32] The leapfrog integration algorithm with a time step of 0.2 fs was used for determination of the equation of motion. The Ewald sum was used for

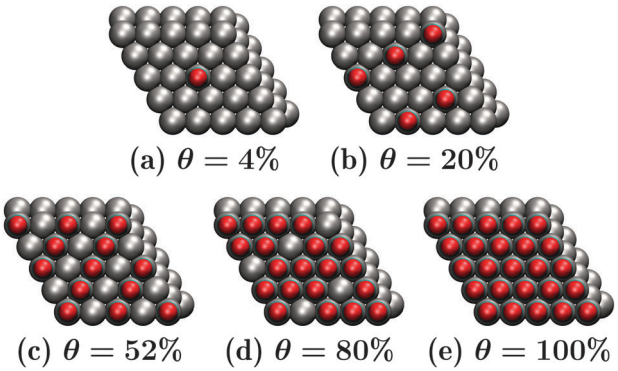

Fig. 1 Quasi-random patterns for different coverages (θ) of CO adsorbed on Pt(111) surfaces. (a) θ = 4%, (b) θ = 20%, (c) θ = 52%, (d) θ = 80%, (e) θ = 100%.

calculating the electrostatic interactions.[33] The cutoff radius was set to be 6 Å in MD simulations due to the length of the periodic box. The large surface area used here is comparable with that in the previous study[34] and can partially exclude the artifact of PBC.[28] After equilibrium, another 100 ps MD production simulations were performed.

In present MD simulations, the Pt–Pt interaction was represented by the Sutton–Chen potential.[35] The effective Lennard-Jones parameters σ_{eff} and ε_{eff} for Pt, which were only used to evaluate the cross interactions of Pt–water by Lorentz–Berthelot mixing rules, were chosen to be 2.41 Å and 4.645 kcal mol^{-1}, respectively.[36] Meanwhile, geometrical parameters of water molecules were constrained at the optimized geometries of the SPC[37] force field by the SHAKE algorithm.[38] The C–O bond and the Pt–C–O angle were described as harmonic potential at the B3LYP level with an equilibrium bond length of 1.150 Å, a force constant of 17.4 mdyn Å^{-1}, and an equilibrium bond angle of 180°, a force constant of 0.43 mdyn Å rad^{-2}, respectively.[39] During MD simulations, the positions of two bottom Pt(111) slab layers were fixed to mimic the bulk electrodes. All CO molecules were fixed on the atop sites by harmonic potential between the Pt and C atoms with an equilibrium bond length of 1.787 Å and a force constant of 5.1 mdyn Å^{-1}.[39] There are two advantages of fixing CO on the atop sites. One is to circumvent the CO "puzzle" for DFT calculations since the DFT–GGA methods overestimate the adsorption energy (AE) of CO on the hollow sites.[40] The other is to eliminate the systematic error for AE of CO adsorbed on Pt(111) surfaces at the DFT level.[41] Although CO molecules will be adsorbed not only on the top sites but also on other sites at high coverages, we neglected the contribution from CO adsorbed on the other sites for simplification since experimental results show that the proportion of these CO molecules is small.[21,42]

The Lennard-Jones parameters for CO molecules were taken from the Amber parm99 parameter set.[43] It has been shown that the dipole moment of CO is small and the WF of the Pt(111) surface changed a little after adsorption of CO molecules.[23,44] As a result, Pt atoms and CO molecules were set to be neutral. The validity of all intermolecular interactions except the water–CO was evaluated for generating reliable structures in our previous studies.[28] Here, our test calculations also

confirmed that the calculated water–CO structures at the current level are quite similar to those at the *ab initio* level (see ESI† for details). All MD simulations were carried out by using the DL_POLY code.[45]

300 conformations in the last 60 ps of MD trajectories were selected at an interval of 0.2 ps. Based on these configurations, single-point energy calculations at the first principles level were performed for WFs and AEs.[29] The projector augmented-wave (PAW) method was used for core electrons,[46,47] and the wave functions were expanded in a plane-wave basis set with an energy cutoff of 400 eV. The PAW potential was generated with scalar relativistic corrections taken into account. For the *k*-point sampling, a 3 × 3 × 1 mesh of Monkhorst–Pack grid was used, which generates 5 *k* points in the irreducible Brillouin zone, for the Brillouin zone integration.[48] The dipole correction was also employed in the DFT calculations.[49,50] For pure CO/Pt(111) systems in a vacuum, CO molecules and the uppermost Pt slab layer were allowed to relax in the *z*-axis. The final forces on these atoms were less than 0.02 eV Å^{-1}.

The WF is defined as the energy difference between the Fermi level and the vacuum.[51] Meanwhile, the calibrated WF is calculated by

$$\mathrm{WF_{cali}} = \mathrm{WF}_i - \mathrm{WF_{Pt(111)}} + 5.85 \quad (1)$$

where WF_i and $\mathrm{WF_{Pt(111)}}$ are the calculated WFs for the interface and the pure Pt(111) surface in the same configuration. In eqn (1), the experimental WF of the pure Pt(111) surface is set to be 5.85 eV.[52] The AE for different θ is defined as

$$E_{\mathrm{ads}} = -\frac{E_{\mathrm{tot}} - E_{\mathrm{Pt}} - n_{\mathrm{CO}}E_{\mathrm{CO}}}{n_{\mathrm{CO}}}, \quad (2)$$

where n_{CO} represents the number of CO molecules, E_{CO} the energy of a CO molecule in a vacuum. Here E_{tot} is the energy of CO/Pt(111) in a vacuum (or the average energy of water–CO/Pt(111) in EDL), while E_{Pt} is the energy of Pt(111) (or the average energy of water–Pt(111)). For statistical analysis, the standard deviation σ used in this study is the root mean square deviation and can be expressed as[53]

$$\sigma = \sqrt{\frac{1}{N}\sum_i (P_i - \langle P\rangle)^2}, \quad (3)$$

where P_i is the individual calculated property, $\langle P\rangle$ is the average calculated property, and N is the number of calculated property. All the first principles calculations were performed at the DFT level with PBE functional by using the VASP code.[54]

3 Results and discussion

3.1 MD Results

Calculated from the MD trajectories, the average atomic densities within the *x*–*y* plane along the *z*-axis of the oxygen in CO and in water, *i.e.* ρ_z(OC) and ρ_z(W), are depicted in Fig. 2. The results show that ρ_z(W) in the outermost layer of water for different θ are all up to the density of bulk water, which indicates that the number of water molecules is sufficient in our simulations, as confirmed also in our previous study.[28] By the inspection of Fig. 2, it can be seen that the ρ_z behavior can be classified into two categories for different θ. One is the wetting situation, *i.e.* θ equals 4% and 20%, in which ρ_z(W) and ρ_z(OC) have an obvious overlap. This result shows that the water molecules can be co-adsorbates of the specifically

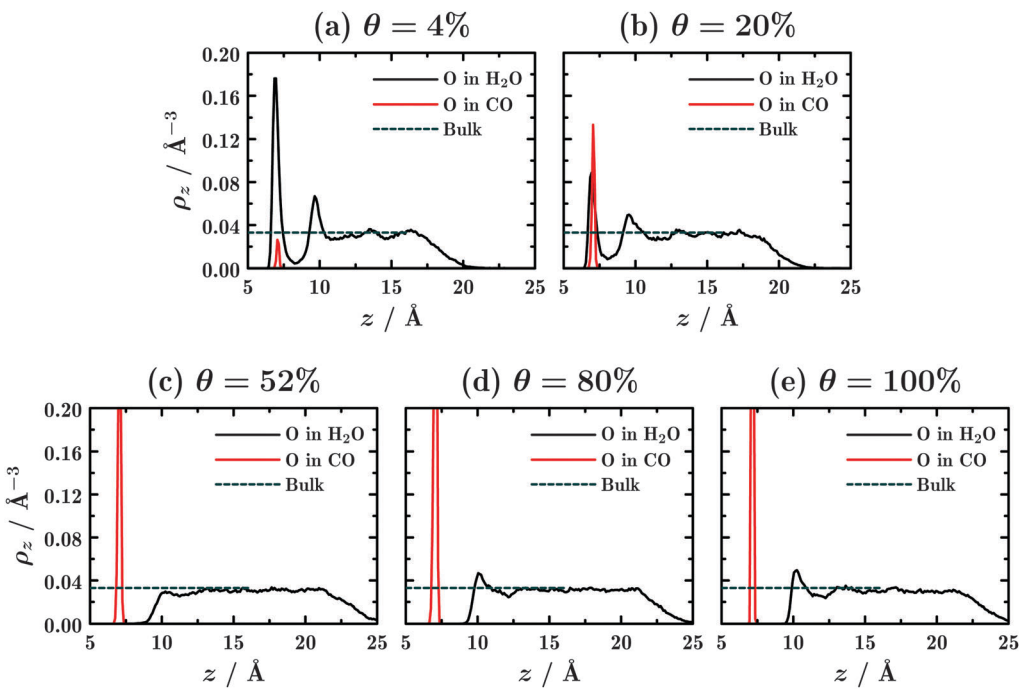

Fig. 2 ρ_z of oxygen atoms for different coverages (θ) of CO adsorbed on Pt(111) surfaces. (a) θ = 4%, (b) θ = 20%, (c) θ = 52%, (d) θ = 80%, (e) θ = 100%. Black solid and red solid lines represent the ρ_z of oxygen in water and in CO respectively. The dark cyan dashed line indicates the density of bulk water at room temperature.

adsorbed CO molecules. Furthermore, the first peak positions of ρ_z(W) and ρ_z(OC) are almost the same in this situation, which reveals that the water–CO interaction in the first solvation layer is important in EDL. The other is the non-wetting situation, *i.e.* θ equals 52%, 80% and 100%, where there is no overlap between ρ_z(W) and ρ_z(OC). On the other hand, the position of the first peak in ρ_z(W) has shifted to larger separation as θ increases, which indicates that there exists a repulsion interaction between water and the CO/Pt(111) surface especially at high θ and also a ''competition'' adsorption between water and the specifically adsorbed CO molecules on Pt(111) surfaces in the first solvation layer. Interestingly, for CO and water in a vacuum, this kind of interaction is attractive (see ESI† for details). Typical snapshots of CO adsorbed on Pt(111) surfaces with different θ are illustrated in Fig. 3, where the mentioned two categories are clearly shown with atomic details. Fig. 3 also shows that the oxygen in CO plays an important role when adsorbed CO molecules interact with water molecules.

The feature of the ρ_z(W) peaks in the first water layer at different θ is also distinguishable, which is illustrated in Fig. 2. In the wetting situation, the peaks are sharp and their intensities decrease as θ increases, whereas in the non-wetting cases, the peaks behave completely different: they are broad and their intensities increase as θ increases. It is known that the sharper the peak is, the stronger the interaction with the surfaces exists.[28] The decreased ρ_z(W) peak intensity along with the increase of θ under the wetting conditions confirms that the interactions between CO and water at the interface are repulsive since the interactions between Pt(111) and water with no CO present are attractive.[28] In this situation, the overall interactions between water and CO/Pt(111) surfaces are still attractive. Meanwhile, the increased ρ_z(W) peak intensity in the first water layer with higher θ under the non-wetting conditions reveals that the overall interactions between water and CO/Pt(111) surfaces are repulsive and become stronger with the increase of θ. It is noteworthy that when θ equals 52%, there is no obvious peak appearing in ρ_z(W). In this situation, the decay of ρ_z(W) in the first water layer and the outermost layer is quite similar, which implies that the force on the first water layer could be virtually zero. Thus, it can be estimated that the critical point between attractive and repulsive interaction of the water molecules and the CO/Pt(111) surfaces is around 52%.

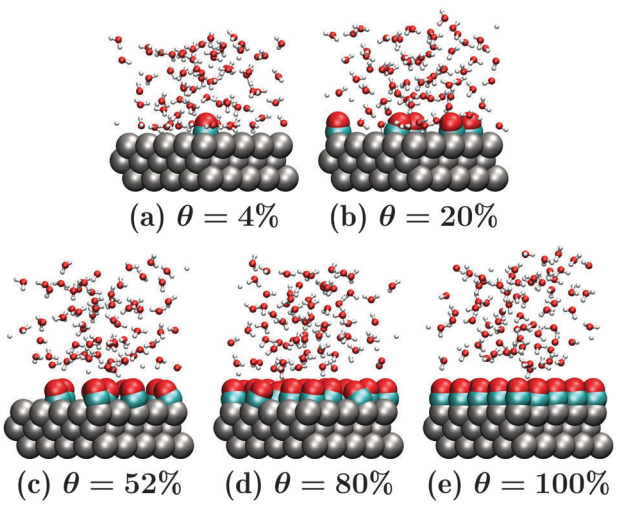

Fig. 3 Typical snapshots for different coverages (θ) of CO adsorbed on Pt(111) surfaces. (a) θ = 4%, (b) θ = 20%, (c) θ = 52%, (d) θ = 80%, (e) θ = 100%.

3.2 The first principles results in a vacuum

Although classical MD simulations can predict the dynamic structures quite well, the electronic properties still need to be solved by using the high-level first principles methods. The calculated WFs and AEs of CO/Pt(111) systems in a vacuum under different θ are listed in Table 1 with the adsorption patterns shown in Fig. 1. The optimized Pt–C bond length at different θ is all around 1.86 Å, consistent with the results of previous theoretical calculations.[22]

Due to the use of PBC, WFs of the CO/Pt(111) surface and the pure Pt(111) surface can be calculated simultaneously for each pattern. When there is no CO adsorbed, *i.e.* θ equals 0%, the calculated WFs for both sides are 5.85 eV for the pure Pt(111) surface, which is in good agreement with experimental measurements.[52,55,56] This consistency shows that the current DFT functional (PBE) is accurate enough to calculate WFs for the CO/Pt(111) systems. When θ increases, the calculated WFs for the pure Pt(111) surface show a decreasing tendency. This indicates that the adsorbed CO molecules do have some influences on the properties of the back layer, *i.e.* the pure Pt(111) surfaces, due to the thin Pt slab layer used. Nevertheless, the largest deviation from the unperturbed WF for the pure Pt(111) is only 0.15 eV, ensuring the reliability of the three slab layers in the current work (see ESI† for details). In fact, the calculated WF of the pure Pt(111) surface for each pattern can be used to calibrate that of the CO/Pt(111) surface with exclusion of the influences of finite Pt layers using eqn (1). The calibrated WFs of the CO/Pt(111) surfaces at different θ are depicted in Fig. 4. When θ increases from 0% to 50%, the calibrated WFs slightly decrease. The largest decrease is 0.21 eV at 50% coverage, which is in good agreement with experimental observation (0.23 eV).[23] With a further increase of θ, the calibrated WF increases and is close to that of the pure Pt(111) surface. This is consistent with the trends observed by experiments. However, there are slight differences at high values of θ. For instance, WF drops are 0.13 and −0.02 eV in

Table 1 Calculated work functions (WFs) and adsorption energies (AEs) in eV of CO/Pt(111) systems under different CO coverages (θ) in a vacuum at the DFT level

	WF		
θ	Calculated	Calibrated[a]	AE
0	5.85	5.85	0.00
4	5.82	5.80	1.79
20	5.61	5.66	1.77
52	5.52	5.64	1.41
80	5.63	5.78	1.12
100	5.72	5.87	0.94

[a] Calibrated using eqn (1).

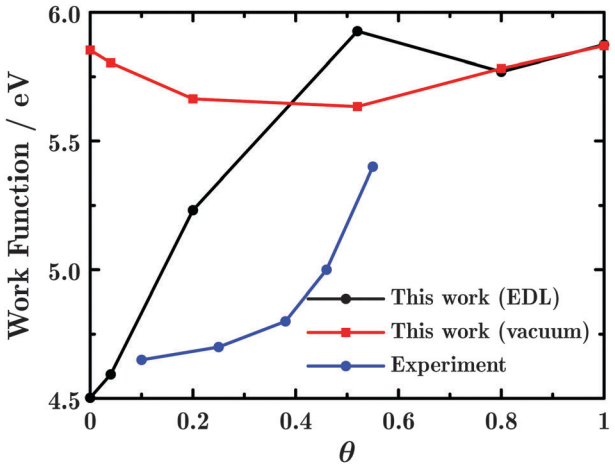

Fig. 4 The calculated work functions (WFs) at different CO coverages. The black circle and red square lines represent the averaged WFs of the CO/Pt(111) interface immersed in water and the WFs in a vacuum, respectively. In order to compare, the experimental data[21] of CO and water co-dosed onto Pt(111) at 110 K under ultrahigh vacuum are also shown with the blue circle line.

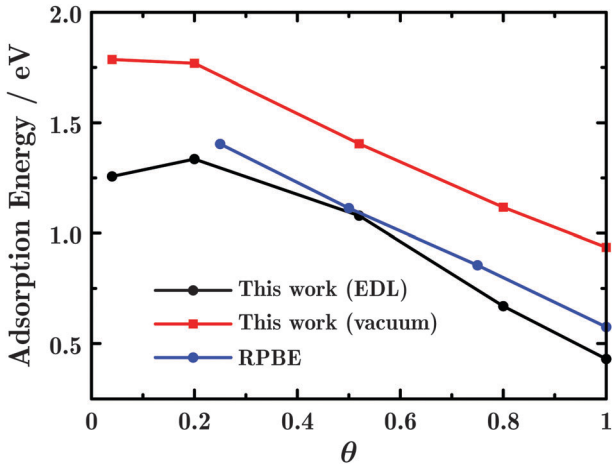

Fig. 5 The calculated adsorption energies at different CO coverages. Black circle and red square lines represent the adsorption energies of the CO/Pt(111) interface immersed in water and in a vacuum respectively. Blue circle line shows the RPBE results extracted from ref. 22.

the experimental measurements and current calculations respectively.[23] In principle, the WF can be calculated as[9]

$$\mathrm{WF} = D - \bar{\mu}, \quad (4)$$

where $\bar{\mu}$ is the position of the Fermi level relative to the average potential in the interior of the crystal and D is the surface-dipole potential. As a result, WF drops are equivalent to the surface-dipole. Therefore, the small decrease in WF indicates that the surface dipole in the CO/Pt(111) systems can be neglected, which confirms that the choice of neutral charges of C and O atoms in CO molecules in the current MD simulation is reasonable. This result is consistent with other theoretical conclusions.[57,58]

Our calculated AEs are listed in Table 1. AE increases with the decrease of θ and is converged around 1.8 eV. This converged value is in the range of experimental observations that reported from 1.41 to 1.90 eV.[59–63] We also notice that our calculated AEs with PBE functional are systematically higher than the previous theoretical results with RPBE functional when θ is larger than 20%.[22] We plotted both results for different functionals in Fig. 5. Comparing our (the red square line) and previous (the blue circle line) calculated results, one can see a systematic discrepancy around 0.4 eV from the difference in functionals. We also found that, in Fig. 5, the slopes of both results are almost the same, revealing that both functionals have the comparable capability to describe the repulsive interactions between adsorbed CO molecules. A previous study has shown that the RPBE functional is particularly useful for describing the intermolecular interactions.[22] In this context, the performance of the PBE functional for the repulsion between adsorbed CO molecules should be also very reliable.

3.3 The first principles results under EDL conditions

We have used water–CO/Pt(111) as a model to mimic the system with CO specifically adsorbed on the Pt(111) electrode in extremely dilute solution. The focus of the study is to explore the effect of room temperature on the interfacial properties, which is done using evenly selected configurations from MD trajectories.

The calculated average WF (AWF) of the water–CO/Pt(111) system and its statistical behavior from PBE functional are listed in Table 2. As discussed above, there are two possible WFs for each configuration. One is related to the pure Pt(111) surface and the other to the water–CO/Pt(111) surface. It is noted that the latter corresponds to the electrode potential of Pt(111) electrodes with different θ.

The calculated AWFs of the pure Pt(111) surfaces from MD configurations with different θ are all around 5.60 eV which agrees well with the experimental measurements of 5.85 eV.[52] On the other hand, the σ of the calculated WFs for the pure Pt(111) surfaces under all θ are small and less than 0.02 eV, which manifests that the configuration changes of water and CO molecules on one side of the water–CO/Pt(111) interface have little influence on the other side, implying that the Pt slab is thick enough for present investigations. In addition, the calculated AWFs of the pure Pt(111) surfaces can also be used for calibrating the calculated WFs of the water–CO/Pt(111) surfaces by eqn (1).

Table 2 Calculated average (Aver.), maximum (Max.) and minimum (Min.) work functions (in eV) for water–CO/Pt(111) and Pt(111) systems under different CO coverages (θ), together with standard deviation (σ)

	Water–CO/Pt(111)				Pure Pt(111)	
θ	Aver.[a]	σ	Max.	Min.	Aver.	σ
0	4.26(4.51)	0.56	6.00	2.69	5.60	0.01
4	4.35(4.59)	0.62	6.04	2.38	5.61	0.01
20	4.96(5.23)	0.62	6.63	3.54	5.58	0.02
52	5.67(4.93)	0.57	6.78	4.04	5.59	0.01
80	5.55(5.77)	0.61	6.75	3.87	5.63	0.02
100	5.65(5.88)	0.57	7.04	3.82	5.62	0.02

[a] Calibrated WFs are in parentheses.

In contrast to pure Pt(111) surfaces, the calculated AWFs of water–CO/Pt(111) surfaces are changed significantly with θ and can be classified into two categories. The critical point of these two categories corresponds to θ of 52%, which is also the critical point for co-adsorption of CO and water. The calculated AWFs of the water–CO/Pt(111) surfaces calibrated by that of the pure Pt(111) surfaces are shown in Fig. 4 using the black circle line. When θ is less than 52%, the calibrated AWFs increase from 4.50 eV to slightly larger than the WF of pure Pt(111) surfaces with the increase of θ. At the same θ, the calculated WFs of the CO/Pt(111) surfaces in a vacuum only slightly decreased by 0.21 eV. This result demonstrates that the adsorbed water molecules have significantly polarized the Pt(111) electrode. Compared with the experimental measurements[21] depicted in Fig. 4 with the blue circle line, the theoretical modeling provides the same trend of the increasing WF with the increasing θ, although some discrepancies between the specific values do exist. The discrepancies probably reflect the different situations between the theoretical modeling and the experimental system. For instance, the small proportion of CO adsorbed on bridge sites observed in experiments[21] was completely neglected in theoretical simulations. We anticipate that, if the CO molecules are not fixed on the top sites, a better agreement between simulations and experiments could be obtained. However, in the framework of our simulations, a more accurate/quality force field of the interaction between CO and Pt(111) surfaces is required for this kind of simulations. When θ is larger than 52%, the calibrated AWFs slightly decrease towards the WF of the pure Pt(111) surface and are almost the same as the calculated WFs of the CO/Pt(111) surface in a vacuum. This is consistent with the fact that there are only CO adsorbed on Pt(111) surfaces and all water molecules are screened by CO molecules. Or in other words, the water molecules are far away from the Pt(111) surface and cannot significantly polarize the electrode anymore. Here, we should emphasize that this conclusion is only for averaged WFs. The situation of instantaneous WFs is completely different (see following discussion).

The σ's of the calculated WFs of the water–CO/Pt(111) surfaces shown in Table 2 are also different from those of the pure Pt(111) surfaces. In general, the value of σ for the calculated WFs of the water–CO/Pt(111) surfaces is around 0.6 eV. This result is caused by the thermal motion of the water molecules since CO molecules do not affect the interfacial WF too much as discussed before.

After calibrated by the WFs of pure Pt(111), we can plot the histogram distribution of the calculated WFs of the water–CO/Pt(111) surfaces with different θ shown in Fig. 6. Under the wetting conditions, the histogram distributions appear as a normal distribution, where the calibrated AWFs are approximately shown in the center, as illustrated in Fig. 6(a)–(c). Meanwhile, under the non-wetting conditions, the histogram distributions are no longer normal and give a feature of low WF tail especially in Fig. 6(e) and (f). According to the definition of WF,[51] the broad distributions reveal essentially high electrochemical activities. When the instantaneous WF fluctuates to a lower value, the electron in the Fermi level which always locates in the energy band of Pt slabs can be released easily. Therefore, the reduction reaction near the CO/Pt(111) electrode should be benefited in this situation. Meanwhile when the instantaneous WF fluctuates to a higher value, the oxidation reaction is much favorable. Similar to the previous study, we believe that this feature at least exists at the nanoscale.[28] It should be pointed out that the time resolution of such broad distributions for the instantaneous WFs is less than 20 ps in the simulation, which might not be detected by conventional experimental

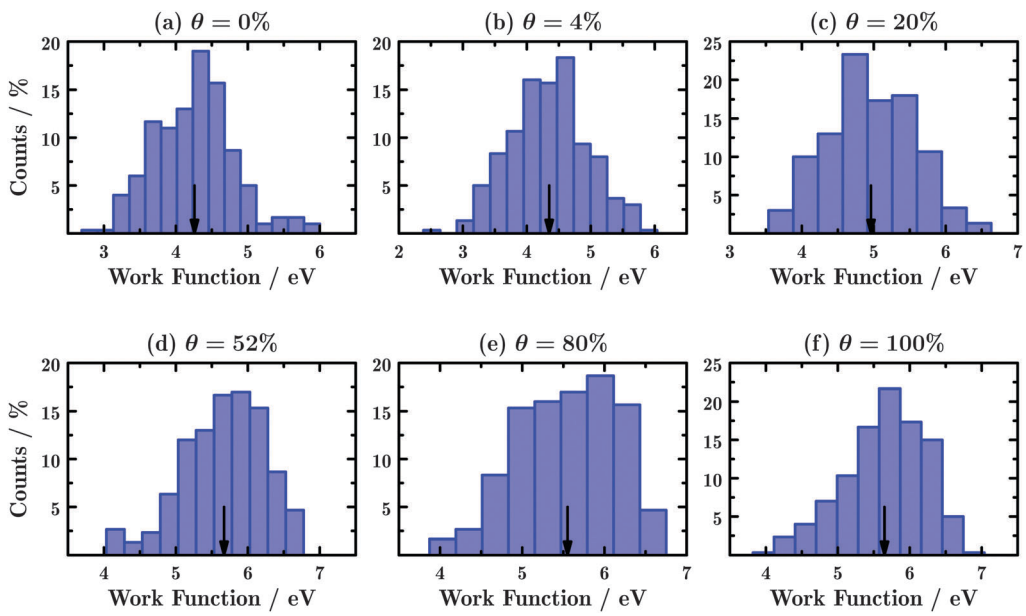

Fig. 6 Statistical histogram of the calculated work functions for the water–CO/Pt(111) interface at room temperature under different CO coverages (θ). (a) θ = 0%, (b) θ = 4%, (c) θ = 20%, (d) θ = 52%, (e) θ = 80%, (f) θ = 100%. The arrows indicate the average value of the calculated work functions.

Table 3 Calculated average (Aver.), maximum (Max.) and minimum (Min.) adsorption energies (in eV) for water–CO/Pt(111) systems under different CO coverages (θ), together with standard deviation (σ)

θ	Aver.	σ	Max.	Min.
4	1.25	1.29	6.00	−2.44
20	1.33	0.24	2.07	0.62
52	1.08	0.09	1.42	0.70
80	0.67	0.06	0.83	0.47
100	0.43	0.05	0.57	0.26

equipment. However, since the time scale of electron transfer is in the region of femtoseconds,[64] the fluctuations of WF can thus affect the electrochemical reactions in the interface at least at the nanoscale. Recently, the dynamic aspect of the chemical activity of the nano-electrode has been predicted both theoretically and experimentally.[65,66]

We also calculated AEs of CO and their statistical behaviors based on MD configurations with different θ by eqn (2) and the results are presented in Table 3. The largest average AE (AAE) occurs when θ equals 20%. Usually, AE increases along with the decrease of θ in a vacuum. This result thus reveals that the surrounding water molecules can screen the repulsive interaction between the adsorbed CO molecules. In fact, this screening effect can also be reflected by the slope change around the critical point shown in Fig. 5. For instance, the small slope at the side in wetting conditions should owe to this effect. The calculated AAEs are systematically less than the AEs in a vacuum, which is shown in Fig. 5. The systematical difference between them is around 0.4 eV. The reason accounting for this difference could be that the equilibrium bond length of Pt–C used in MD simulation is 1.787 Å,[39] which is shorter than the optimized values in a vacuum (around 1.86 Å). How to bridge this difference is beyond our computational capacity. In principle, the long time-scale first principles MD simulation could be an alternative toward this end. Obviously, one cannot rule out the possible effect of the surrounding water molecules on such a difference.

The histogram distributions of the calculated AEs in Fig. 7 show normal behavior. We also notice that σ of AEs decreases from 1.29 to 0.05 eV along with increasing θ. This is mainly ascribed to the fact that the fluctuation of AEs will be canceled by the thermal motion of the adsorbed CO molecules. It turns out that σ is almost inversely proportional to θ as shown in Table 3. Another reason is that the water molecules are excluded by adsorbed CO at larger θ and their effect on the CO thermal motion decreases. On the other hand, the adiabatic description of AE in eqn (2) shows that the energy changes of water molecules are also included in the σ of AEs. This can cause some artifacts in the fluctuations of AEs. For instance, the obvious probability of AE less than zero at θ equal to 4% has been predicted.

4 Conclusions

In the present work, we have investigated CO molecules adsorbed on atop sites of Pt(111) surfaces with different CO coverages either in a vacuum or immersed in water using combined classical MD and DFT techniques. The temperature effect was considered by classical MD simulations. The WF and AE were calculated at the first principles level based on the configurations extracted from the MD trajectories.

According to the MD trajectories, we found that a critical point, where CO was adsorbed on half monolayer, existed between the wetting and non-wetting situations. This is the result of the competitive adsorption of CO and water molecules

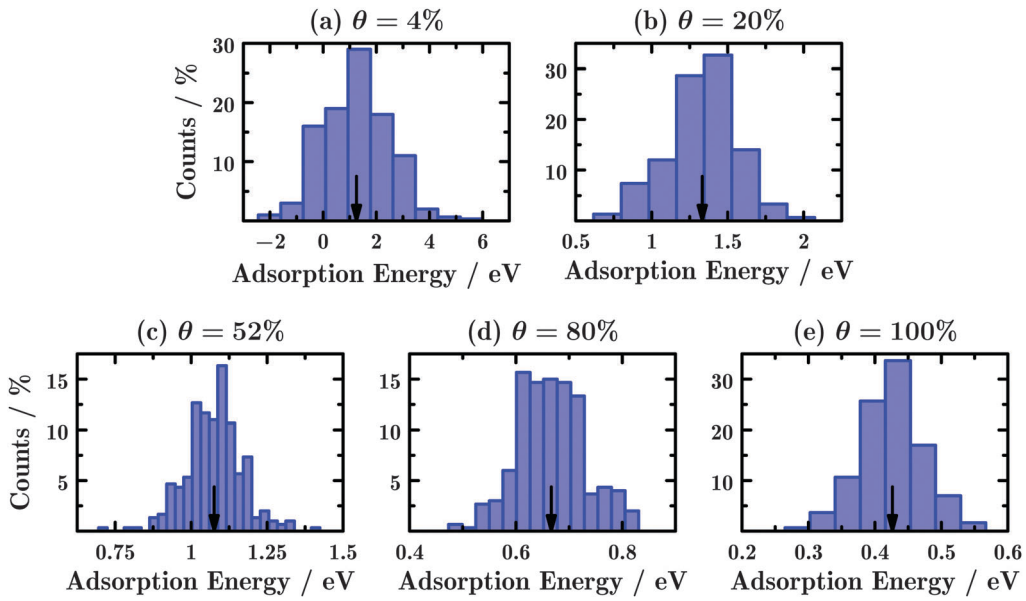

Fig. 7 Statistical histogram of first principles calculated adsorption energies for the water–CO/Pt(111) interface at room temperature under different CO coverages (θ). (a) θ = 4%, (b) θ = 20%, (c) θ = 52%, (d) θ = 80%, (e) θ = 100%. The arrows indicate the average value of the calculated adsorption energies.

on the Pt(111) surface. At the critical point, the force on the water molecules from the CO/Pt(111) surface virtually disappeared, and then, a novel structure of water molecules formed.

The calibrated AWFs of the water–CO/Pt(111) systems increase along with the increase of the CO coverage θ until it reaches the critical point, and this finding agrees with the experimental observations.[21] Under the critical point, AWFs are significantly different from WFs of the CO/Pt(111) surfaces in a vacuum due to the polarization of the Pt(111) surface by water molecules, while when θ increases beyond the critical point, AWFs become close to WFs of the CO/Pt(111) surfaces since the water molecules in the first solvent shell are blocked out by the adsorbed CO molecules. The σ's of the calculated WFs for the water–CO/Pt(111) surfaces are all around 0.6 eV. Meanwhile, the critical point for the feature of WFs' distribution is also around 50%.

The critical point is also distinguished by the different slopes of the calculated AAEs of CO with respect to θ. In contrast to the calculated WFs, σ of the calculated AEs monotonously decreased with the increasing θ. This is caused by the cancellation of the thermal motion in the different adsorbed CO molecules.

The results presented in this work should be beneficial for the understanding of the geometrical and electronic properties of the water–CO/Pt(111) interface with atomic details and also for the design of electrochemical catalysts based on the Pt electrode. Finally, we also believe that our proposed method that combines the classical MD simulations for structures and the first principles methods for electronic properties can be widely used for investigating other electrochemical interfaces.

Acknowledgements

This work was supported by the Ministry of Science and Technology (2009CB930703, 2010CB923300, and 2011CB808505), the Natural Science Foundation of China (Grants 20973143 and 20925311), and the Göran Gustafsson Foundation for Research in Natural Sciences and Medicine. The high performance computational center of Xiamen University and the Swedish National Infrastructure for Computing (SNIC) are acknowledged for computer time.

References

1 D. Pletcher and F. C. Walsh, *Industrial Electrochemistry*, Springer-Verlag, New York, 2nd edn, 1990.
2 *Bioelectrochemistry: Fundamentals, Experimental Techniques and Applications*, ed. P. N. Bartlett, John Wiley & Sons Ltd, Chichester, 1st edn, 2008.
3 A. J. Bard and L. R. Faulkner, *Electrochemical Methods: Fundamentals and Applications*, Wiley, New York, 2nd edn, 2001.
4 *Structure of Electrified Interfaces*, ed. L. Lipkowski and P. H. Ross, VCH Publishers, Weinheim, 1993.
5 B. Meyer, D. Marx, O. Dulub, U. Diebold, M. Kunat, D. Langenberg and C. Wöll, *Angew. Chem., Int. Ed.*, 2004, **43**, 6642–6645.
6 H. L. F. von Helmholtz, *Pogg. Ann.*, 1853, **89**, 211–233.
7 D. M. Kolb, *Angew. Chem., Int. Ed.*, 2001, **40**, 1162–1181.
8 J. O. Bockris, M. A. V. Devanathan and K. Muller, *Proc. R. Soc. London, Ser. A*, 1963, **274**, 55–79.
9 A. Y. Lozovoi, A. Alavi, J. Kohanoff and R. M. Lynden-Bell, *J. Chem. Phys.*, 2001, **115**, 1661–1669.
10 J. S. Filhol and M. Neurock, *Angew. Chem., Int. Ed.*, 2006, **45**, 402–406.
11 Y. H. Fang and Z. P. Liu, *J. Phys. Chem. C*, 2009, **113**, 9765–9772.
12 J. Rossmeisl, E. Skúlason, M. E. Björketun, V. Tripkovic and J. K. Nørskov, *Chem. Phys. Lett.*, 2008, **466**, 68–71.
13 J. K. Nørskov, J. Rossmeisl, A. Logadottir, L. Lindqvist, J. R. Kitchin, T. Bligaard and H. Jónsson, *J. Phys. Chem. B*, 2004, **108**, 17886–17892.
14 J. A. Keith, G. Jerkiewicz and T. Jacob, *ChemPhysChem*, 2010, **11**, 2779–2794.
15 W. Gao, J. A. Keith, J. Anton and T. Jacob, *J. Am. Chem. Soc.*, 2010, **132**, 18377–18385.
16 R. Jinnouchi and A. B. Anderson, *Phys. Rev. B: Condens. Matter Mater. Phys.*, 2008, **77**, 245417.
17 Y. H. Fang and Z. P. Liu, *J. Am. Chem. Soc.*, 2010, **132**, 18214–18222.
18 Y. X. Chen, M. Heinen, Z. Jusys and R. J. Behm, *Angew. Chem., Int. Ed.*, 2006, **45**, 981–985.
19 S. Uhm, H. J. Lee, Y. Kwon and J. Lee, *Angew. Chem., Int. Ed.*, 2008, **47**, 10163–10166.
20 J. J. Baschuk and X. Li, *Int. J. Energy Res.*, 2001, **25**, 695–713.
21 N. Kizhakevariam, X. Jiang and M. J. Weaver, *J. Chem. Phys.*, 1994, **100**, 6750–6764.
22 B. Shan, Y. Zhao, J. Hyun, N. Kapur, J. B. Nicholas and K. Cho, *J. Phys. Chem. C*, 2009, **113**, 6088–6092.
23 M. Kiskinova, G. Pirug and H. P. Bonzel, *Surf. Sci.*, 1983, **133**, 321–343.
24 X. Q. Gong, P. Hu and R. Raval, *J. Chem. Phys.*, 2003, **119**, 6324–6334.
25 J. G. Wang and B. Hammer, *J. Chem. Phys.*, 2006, **124**, 184704.
26 J. Bergeld, B. Kasemo and D. V. Chakarov, *Surf. Sci.*, 2001, **495**, L815–L820.
27 M. Kinne, T. Fuhrmann, J. F. Zhu, B. Tränkenschuh, R. Denecke and H. P. Steinrück, *Langmuir*, 2004, **20**, 1819–1826.
28 S. Duan, X. Xu, Z.-Q. Tian and Y. Luo, *Phys. Rev. B: Condens. Matter Mater. Phys.*, 2012, **86**, 045450.
29 J. P. Perdew, K. Burke and M. Ernzerhof, *Phys. Rev. Lett.*, 1996, **77**, 3865–3868.
30 *CRC Handbook of Chemistry and Physics*, ed. D. R. Lide, Taylor and Francis, Boca Raton, FL, 87th edn, 2007.
31 P. J. Feibelman, B. Hammer, J. K. Nørskov, F. Wagner, M. Scheffler, R. Stumpf, R. Watwe and J. Dumesic, *J. Phys. Chem. B*, 2001, **105**, 4018–4025.
32 W. G. Hoover, *Phys. Rev. A: At., Mol., Opt. Phys.*, 1985, **31**, 1695–1697.
33 M. P. Allen and D. J. Tildesley, *Computer Simulation of Liquids*, Clarendon Press, Oxford, 1989.

34 J. W. Halley, A. Mazzolo, Y. Zhou and D. Price, *J. Electroanal. Chem.*, 1998, **450**, 273–280.
35 A. P. Sutton and J. Chen, *Philos. Mag. Lett.*, 1990, **61**, 139–146.
36 S. Y. Liem and K. Y. Chan, *Mol. Phys.*, 1995, **86**, 939–949.
37 H. J. C. Berendsen, J. P. M. Postma, W. F. van Gunsteren and J. Hermans, *Intermolecular Forces*, Reidel, Dordrecht, 1981, p. 331.
38 J. P. Ryckaert, G. Ciccotti and H. J. C. Berendsen, *J. Comput. Phys.*, 1977, **23**, 327–341.
39 L. Manceron, B. Tremblay and M. E. Alikhani, *J. Phys. Chem. A*, 2000, **104**, 3750–3758.
40 I. Grinberg, Y. Yourdshahyan and A. M. Rappe, *J. Chem. Phys.*, 2002, **117**, 2264–2270.
41 S. E. Mason, I. Grinberg and A. M. Rappe, *Phys. Rev. B: Condens. Matter Mater. Phys.*, 2004, **69**, 161401.
42 F. Dederichs, K. A. Friedrich and W. Daum, *J. Phys. Chem. B*, 2000, **104**, 6626–6632.
43 T. E. Cheatham 3rd, P. Cieplak and P. A. Kollman, *J. Biomol. Struct. Dyn.*, 1999, **16**, 845–862.
44 W. Koch and M. C. Holthausen, *A Chemist's Guide to Density Functional Theory*, Wiley-VCH Verlag GmbH, 2nd edn, 2001.
45 W. Smith, C. W. Yong and R. M. Rodger, *Mol. Simul.*, 2002, **28**, 385–471.
46 P. E. Blöchl, O. Jepsen and O. K. Andersen, *Phys. Rev. B: Condens. Matter Mater. Phys.*, 1994, **49**, 16223–16233.
47 G. Kresse and D. Joubert, *Phys. Rev. B: Condens. Matter Mater. Phys.*, 1999, **59**, 1758–1775.
48 H. J. Monkhorst and J. D. Pack, *Phys. Rev. B: Condens. Matter Mater. Phys.*, 1976, **13**, 5188–5192.
49 J. Neugebauer and M. Scheffler, *Phys. Rev. B: Condens. Matter Mater. Phys.*, 1992, **46**, 16067–16080.
50 G. Makov and M. C. Payne, *Phys. Rev. B: Condens. Matter Mater. Phys.*, 1995, **51**, 4014–4022.
51 C. J. Fall, N. Binggeli and A. Baldereschi, *J. Phys.: Condens. Matter*, 1999, **11**, 2689–2696.
52 T. Pajkossy and D. M. Kolb, *Electrochim. Acta*, 2001, **46**, 3063–3071.
53 L. Råde and B. Westergren, *Mathematics Handbook for Science and Engineering*, Springer-Verlag, Berlin, 5th edn, 2004.
54 G. Kresse and J. Furthmüller, *Phys. Rev. B: Condens. Matter Mater. Phys.*, 1996, **54**, 11169–11186.
55 W. Ranke, *Surf. Sci.*, 1989, **209**, 57–76.
56 M. Kiskinova, G. Pirug and H. P. Bonzel, *Surf. Sci.*, 1985, **150**, 319–338.
57 F. Ample, D. Curulla, F. Fuster, A. Clotet and J. M. Ricart, *Surf. Sci.*, 2002, **497**, 139–154.
58 M. Mamatkulov and J. S. Filhol, *Phys. Chem. Chem. Phys.*, 2011, **13**, 7675–7684.
59 Y. Wang, S. de Gironcoli, N. S. Hush and J. R. Reimers, *J. Am. Chem. Soc.*, 2007, **129**, 10402–10407.
60 H. Steininger, S. Lehwald and H. Ibach, *Surf. Sci.*, 1982, **123**, 264–282.
61 G. Ertl, M. Neumann and K. M. Streit, *Surf. Sci.*, 1977, **64**, 393–410.
62 K. Horn and J. Pritchard, *J. Phys. Colloq.*, 1977, **38**, 164–171.
63 Y. Y. Yeo, L. Vattuone and D. A. King, *J. Chem. Phys.*, 1997, **106**, 392–401.
64 R. R. Dogonadze, A. M. Kuznetsov and V. G. Levich, *Electrochim. Acta*, 1968, **13**, 1025–1044.
65 G. N. I. Clark, G. L. Hura, J. Teixeira, A. K. Soper and T. Head-Gordon, *Proc. Natl. Acad. Sci. U. S. A.*, 2010, **107**, 14003–14007.
66 I. Agyekum, C. Nimley, C. Yang and P. Sun, *J. Phys. Chem. C*, 2010, **114**, 14970–14974.